# Can cheniers protect mangroves along eroding coastlines? – The effect of contrasting foreshore types on mangrove stability

Celine E.J. van Bijsterveldt [a,b,*], Daphne van der Wal [a,c], Alejandra Gijón Mancheño [d], Gregory S. Fivash [a], Muhammad Helmi [e], Tjeerd J. Bouma [a,b]

[a] NIOZ Royal Netherlands Institute for Sea Research, Department of Estuarine and Delta Systems, P.O. Box 140, 4400 AC Yerseke, the Netherlands
[b] Faculty of Geosciences, Department of Physical Geography, Utrecht University, P.O. Box 80.115, 3508 TC Utrecht
[c] Faculty of Geo-Information Science and Earth Observation (ITC), University of Twente, P.O. Box 217, 7500 AE, Enschede, the Netherlands
[d] Faculty of Civil Engineering and Geosciences, Department of Hydraulic Engineering, Delft University of Technology, Stevinweg 1, 2628 CN, Delft, the Netherlands
[e] Faculty of Fisheries & Marine Sciences, Oceanography Department, Universitas Diponegoro, Semarang 50275, Indonesia

## ARTICLE INFO

## ABSTRACT

Mangrove forests are increasingly valued as wave-attenuating buffers in coastal flood defence strategies. However, as mangroves are vulnerable to wave-induced erosion, this raises the question, how can the stability of these protective mangrove forests be promoted? To address this question, we investigate how mangrove dynamics in a microtidal system can be related to different types of foreshores. We used remote sensing to investigate mangrove fringe stability over multiple years in relation to intertidal mudflat width (i.e., emerged at low tide) and the presence stability of cheniers, which are sand bodies on top of muddy foreshores that are characteristic for eroding coastlines. In addition, we investigated local and short-term foreshore effects by measuring wave propagation across two cross-shore transects, one with a mudflat and chenier and one with a deeper tidal flat foreshore. The satellite images (Sentinel-2) revealed that mangrove dynamics over multiple years and seasons were related to chenier presence and stability. Without a chenier, a mudflat width of 110 m (95%CI: 76–183 m) was required to make mangrove expansion more likely than mangrove retreat. When a stable chenier was present offshore for two years or more, a mudflat width of only 16 m (95%CI: 0–43 m) was enough to flip chances in favor of mangrove expansion. However, mangrove expansion remained heavily influenced by seasonal changes, and was highly event driven, succeeding only once in several years. Finally, although mudflat width was a direct driver of mangrove expansion, and could be targeted as such in coastal management, our field measurements demonstrated that cheniers also have an indirect effect on mangrove expansion. These sand banks significantly reduce wave height offshore, thereby likely creating favorable conditions for mudflat accretion landward, and thus mangrove habitat expansion. This makes stabilization - and possibly also the temporary creation - of cheniers an interesting target for mangrove conservation and restoration.

## 1. Introduction

Mangrove ecosystems have been increasingly valued for their ecosystem services in the past few decades (Barbier et al., 2011). Besides traditionally valued services such as viable fisheries, nurseries and water filtering capacity, the use of mangroves for coastal protection has also received attention (Mazda et al., 1997; Temmerman et al., 2013). Mangroves attenuate waves with their dense tree tissues, such as extensive aerial root networks and canopy (Bao, 2011; Horstman et al., 2014; Quartel et al., 2007). Their complex root and branch structures reduce the wave velocity and can decrease wave height by 50% with every additional 100 m of forest (Mazda et al., 2006). The use of mangrove greenbelts for wave impact reduction is therefore often discussed in literature and implemented in coastal zone management (Duarte et al., 2013; Narayan et al., 2016; Othman, 1994; Spalding et al., 2014). However, mangrove vegetation itself is also vulnerable to high wave energy and does not typically occur along exposed coastlines (Chapman, 1976). This "vulnerable protectors" paradox can be easily

overlooked in management discussions debating the ideal width needed to obtain the desired amount of wave reduction on the landward edge of the mangrove forest. As a result, there may be clear specifications on the width of a protective mangrove greenbelt in various countries, but it is not always clear if and how such mangrove width can be sustained. For instance, Indonesia prescribes a mangrove greenbelt for coastal protection to be 130 m times the annual average tidal range (Presidential Decree (Kepres) No. 32/1990), whereas the Philippines uses a minimum width between 50 m and 100 m as guideline for coastal mangroves (R.A. 8550, P.D. 705, P.D. 953). Having such clear restrictions on the required wave-attenuating width of a protective greenbelt, requires tools to manage the mangrove forest width, especially under physically hostile conditions. Only by having an in-depth understanding of the environmental conditions that spark mangrove forest retreat and forest regeneration can we develop the means by which to achieve sustainable and effective forest widths.

Mangroves need an episodically occurring period of calm conditions to establish, a so-called Window of Opportunity (Balke et al., 2011). On a small scale, favorable conditions for natural mangrove establishment are nowadays well understood: mangrove seedlings need a window of opportunity in the form of an inundation-, wave-and erosion-free period to strand, root and anchor themselves to survive the first life stages (Balke et al., 2011). On a larger scale, such calm-and wave free conditions can frequently be found in relatively sheltered areas such as lagoons and estuaries. However, at seaward facing sites, such calm conditions will only occur rarely. That is, the presence of such episodic calm conditions may be expected to be driven by the seasons in combination with the foreshore morphology (van Bijsterveldt et al., 2020). As such, dynamic foreshore structures such as mud-banks, intertidal mudflats with or without chenier-sand-banks may be expected to play an important role in creating windows of opportunity for mangrove establishment. This is exemplified along the coastline of the Guianas, where the mangrove dynamics are dominated by fluid mud banks that originate from the Amazon river, and migrate west-ward along the coast (Augustinus, 1978). Mangroves extend seaward when sheltered by wave-dissipating intertidal mud banks and erode during exposed interbank stages (Anthony et al., 2010). Along the mangrove-mud coast of north Java, similar patterns of mangrove recruitment and mangrove dieback can be found in a relatively patchy and young mangrove forest (van Bijsterveldt et al., 2020). Here however, mud-banks are absent and the foreshore seems to be more dominated by intertidal mudflats with, in some cases, cheniers.

Cheniers, bodies of sand sitting on top of intertidal mudflats, can potentially create shelter for mangrove recruitment along coastlines. However, cheniers are typically described as features of eroding mangrove coasts (Anthony et al., 2010). Sand is supplied in small amounts by rivers (Prost, 1989), but is only formed into cheniers when enough wave energy is present to rework the sediment (Augustinus, 1978). Chenier formation has been observed at locations such as the Red River Delta, Vietnam (Van Maren, 2005), the Mississippi Delta (McBride et al., 2007; Russell and Howe, 1935), China (Liu Cangzi and Walker, 1989), West-Africa (Anthony, 1989), North-Java (Tas et al., 2020; van Bijsterveldt, 2015), Australia (Woodroffe and Grime, 1999), and at the Suriname-Guyana coastline (Anthony et al., 2019; Augustinus, 1989). Along the Suriname coast, the wave-conditions driving chenier formation are typically found during the erosive stages of mud-bank migration, when mangroves are also eroded by the waves (Anthony et al., 2010). Satellite images of the mangrove-mud coasts of Java suggest that cheniers might also be present during periods where parts of the mangroves expand, suggesting that the cheniers may take on a sheltering role, enabling mangrove expansion. However, intertidal mudflats also reduce waves at the coastline, and if they are of sufficient width, they may also provide the physical requirements for mangrove establishment (van Bijsterveldt et al., 2020). In this study, we aim to investigate in depth how foreshore characteristics such as intertidal mudflat width and the presence of cheniers relate to mangrove dynamics. We investigate

this along the coastline of Demak, Central Java, Indonesia on two temporal and spatial scales (Fig. 1): (1) At the scale of the coastal system (i.e. in the order of 10s of kilometers) and yearly timescales, we used satellite-derived data in a Geographical Information System (GIS). (2) On a local and short-term scale (i.e. the order of 100 s of meters and a period of days), we used field derived data.

## 2. Methods

### 2.1. Field study: short-term cross-shore wave transformation with and without chenier

#### 2.1.1. Site description

The coastline of Demak, North Java (Indonesia), is delimited by the city of Semarang in the South, and the Wulan River delta in the north (Fig. 1). Demak experiences a microtidal range of 1 m and a mixed, mainly diurnal, tide (Tas et al., 2020). The local wave conditions are mild during most of the year, except during the NW monsoon between November and March, when significant offshore wave heights reach up to 2 m (Van Domburg, 2018). The coastal area is mostly formed by fine muddy sediment, except for the presence of cheniers along the coast. To investigate the short-term sheltering effect of cheniers on a local scale, we measured wave transformation and erosion in two cross-shore transects that were installed in Demak, Java, Indonesia: one transect with a chenier, and one transect without a chenier (Fig. 2a). The location for the transects was selected in such a way that the hydrodynamic boundary conditions of the two locations was as similar as possible except for the presence of a chenier. Therefore, both transects started at a water depth of approximately 1 m with respect to MSL and were spaced 400 m apart along the coastline. The first transect started 260 m offshore from a chenier (chenier transect) and the second transect started at a similar depth and distance from the shoreline, but without a chenier (exposed transect) (Fig. 2b).

The chenier transect featured two cheniers; one bare sand lens that consisted mostly of fine sand, ranging from 63.5 to 500 μm in grainsize (as measured from sediment samples of the top 3 cm, freeze-dried and analyzed using a Malvern Mastersizer 2000), and one vegetated chenier that consisted of a thin layer of sand on top of mud (Fig. 3). In the field, both cheniers were easy to walk on, although the layer of sand appeared thin. Jumping on top of the sediment caused the sand body to quiver, and when walking towards the landward side of each chenier, the sand became so thin that one could sink through the sand into the underlying mud. Along the seaward edge of the chenier (A2a in Fig. 2 a), a more consolidated mud layer was visible where the chenier sand had been eroded away by waves (Fig. A 1 a & b). A series of transparent cores, taken on the seaward side of the chenier transect for a different project in the dry season preceding this study, revealed that the subtidal foreshore of the chenier transect (roughly between the later placed stations A1 and A2a) consisted of alternate layers of mud and sand (Fig. A 1 c), which seems to support the hypothesis presented in Tas et al. (2022) that cheniers are formed through sediment sorting.

The exposed transect did not have an emerged chenier. However, the foreshore stations of the exposed transect (E1-E2 in Fig. 2 a) showed grainsize distributions with much more sand mixed through the sediment than the stations seaward of the chenier in the chenier transect (A1-A2a in Fig. 2 a). This could indicate that the sediment at these stations were the remnants of an old chenier or the start of a new chenier forming in the exposed transect.

The most landward station of the two transects was situated inside the mangrove forest. The sediment composition inside the mangrove stands of the two transects was very similar with a high silt content (>88%) at all sites (Fig. 3), although the forest stations in the exposed transect also contained fine sand (125–250 μm, 2 ± 0.2%) and very fine sand (62.5–125 μm, 7.6 ± 1.2%), indicating that the mangroves at the fringe of the exposed transect were subjected to more wave energy than the mangroves in the chenier transect.
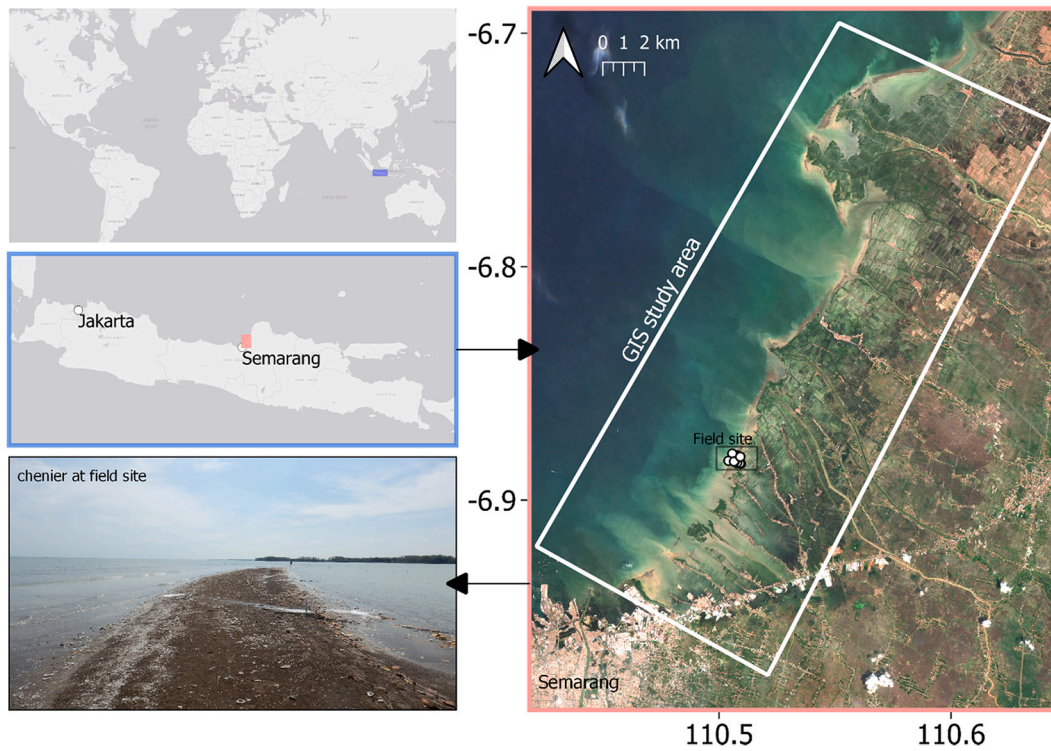
**Fig. 1.** The coastline of Demak district (panel on the right), on the Indonesian island of Java. The two focus areas of this study are indicated by (1) the white box, indicating the focus area of the GIS study in which we studied large scale and long-term chenier effects, and (2) the black rectangle, pinpointing the location of the two cross shore transects in which we studied the small scale and short-term effects of cheniers. The picture in the lower left panel features a chenier in one of the transects, where small waves arrive on the seaward side (left) and distant mangroves are visible on the landward side (right).
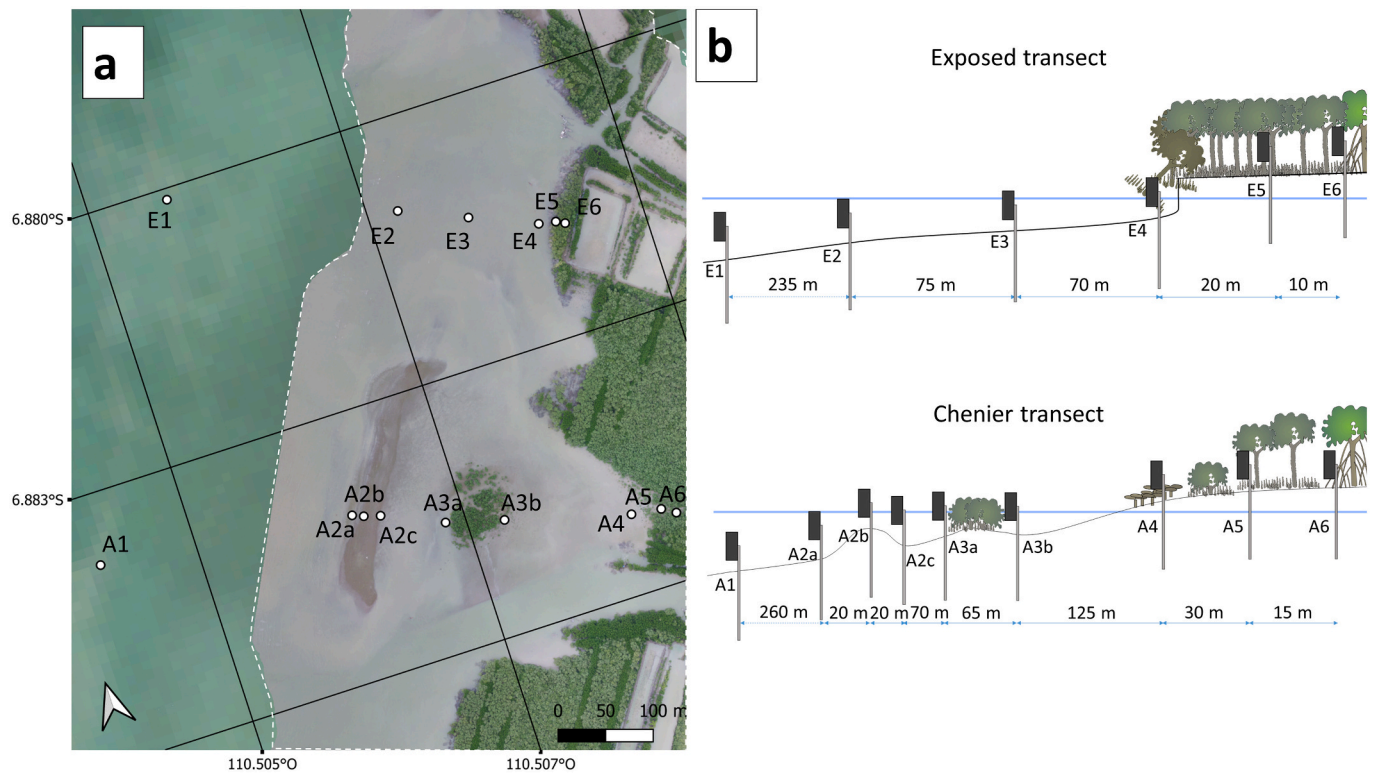


**Fig. 2.** Two cross-shore transects in the field with and without chenier **a**. Wave logger deployment locations are indicated in a drone image (indicated with white dashed outline, a Sentinel-2 image from two weeks later is used in the background) of the transect area in November 2017. The exposed transect did not feature a chenier (E1-E4) and showed mangrove die-back E5-E6. The chenier transect contained a chenier (A2a-A2c), a mangrove stand on an old chenier (A3a-A3b) and a mudflat with seaward expanding mangroves (A4-A6). **b**. Schematized bathymetry and instrument deployment along the exposed and chenier transect.
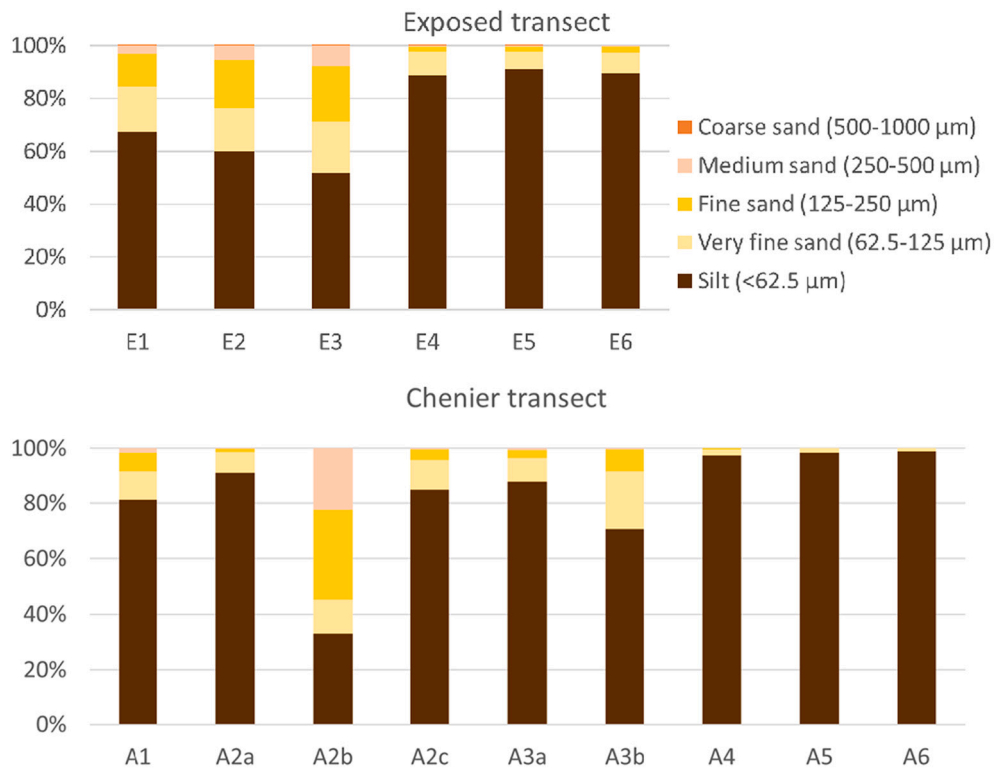
**Fig. 3.** Sediment grainsize distribution at each of the stations in the exposed and chenier transects.

### 2.1.2. Data collection

Wave loggers (OSSI Wave loggers and NIOZ, MARK III SED pressure sensors) were deployed along the two transects at equal distances from the mangrove border in both transects perpendicular to the coast in a north-west direction (Fig. 2b). Additional wave loggers were placed across both the bare and the vegetated chenier in the chenier transect, in order to measure wave propagation across these sheltering landscape features as well. Wave data were collected continuously with a frequency of 10 Hz during 8 days (November 26th-December 4th) during the 2017–2018 wet season, the most turbulent season of the year in terms of onshore waves, storms (MMAF, 2012) and coastal erosion (van Bijsterveldt et al., 2022). While the wet season typically lasts from November until March, the 8-day measurement campaign captured representative wet-season conditions (A 6), and included a storm event that caused extensive flooding of the whole area (Afifah and Hizbaron, 2020). The average significant wave height was therefore determined for both the entire 8-day period, as well as for the storm on the 1st of December, between 00:00 and 05:00, giving insight into the impact of cheniers on average wet-season waves and on extreme storm waves.

Forest parameters were recorded at the landward edge of each transect to typify the forest. We counted the number of seedlings (height < 0.5 m) per species and recorded the diameter at breast height (DBH) of individuals that were larger than 1 m. Individuals between 0.5 m and 1 m in height were recorded as saplings. These species counts and DBH measurements were conducted in circular plots at the most landward station in the exposed and chenier transects after the wet season of 2017–2018. Plot size differed between the exposed and chenier transect (78.5 m^2 and 38.5 m^2 respectively) due to difficulty to move around in the muddy sections of the chenier transect and the risk of trampling seedlings. Forest parameters were therefore corrected to counts per hectare (ha) to compare the two transects.

### 2.1.3. Data analysis

#### 2.1.3.1. Processing hydrodynamic data.
The pressure measurements

from the wave loggers were corrected for the atmospheric pressure, using the air pressure data collected by a wave logger installed in a nearby tree. The offset of each instrument was determined by in-situ calibration: instruments were placed at one location, and water depth was measured manually at different moments of the tidal cycle for validation. After offset correction, the pressure measurements were transformed into water depth assuming a water density of $\rho = 1024$ $kg^{-1}$ $m^3$ and a gravitational acceleration of $g = 9.8$ $m^{-1}$ $s^2$. The mean water levels were derived from the pressure signal, and the detrended pressure signal was then used to calculate the wave density spectra over 19.5-min intervals. The significant wave height (H_m0), and peak period (T_p) were derived from the spectra of each interval. To compare the same wave conditions over the different stations, only those intervals were selected, during which all sensors (also the sensor on top of the chenier) were fully submerged at the same time. The wave heights during these submergence periods were then averaged over the duration of the storm (1st of December) and over the full 8-day measurement period.

### 2.2. GIS study: the relation between intertidal foreshore features and mangrove dynamics

#### 2.2.1. Data collection

To study the effects of cheniers and mudflats on mangroves over multiple years, we performed a GIS study on the coastline of Demak. Sentinel-2 satellite images were selected to study the effect of cheniers because 10 m is the highest resolution of freely available satellite images and a sufficient resolution for the detection of cheniers and changes in mangrove cover. All available Sentinel-2 satellite images during a 4-year period were therefore assessed for cloud cover in the research area and tidal level. Ultimately, only eight images could be selected based on cloud cover (<10%), low tide conditions and season (one post-dry-season and one post-wet season for each year). The exact tidal level at the moment of satellite image acquisition was obtained from a tidal harmonic analysis of the tide station of Semarang. To detect seasonal

changes in mangrove and mudflat dynamics, images were selected based on acquisition dates before the stormy wet season (Dec-Feb) and before the relatively calm season of the year: the dry season (Jun-Aug) and transitional seasons (Mar-May and Sep-Nov).

*2.2.1.1. Image classification.* Satellite images were atmospherically corrected using Sen2cor software. Clouds and cloud shadows were removed from the images by masking QSC values produced by the Sen2Cor software. Then a normalized difference vegetation index (NDVI) band was computed for all selected Sentinel-2 images, and pixels for all bands outside the study area and the zone of interest were masked. The study area was restricted to the region of the tidal flat beginning from the coastal mangrove forest as it appeared in October 2015, reaching 2 km out to sea in a northwest direction from the
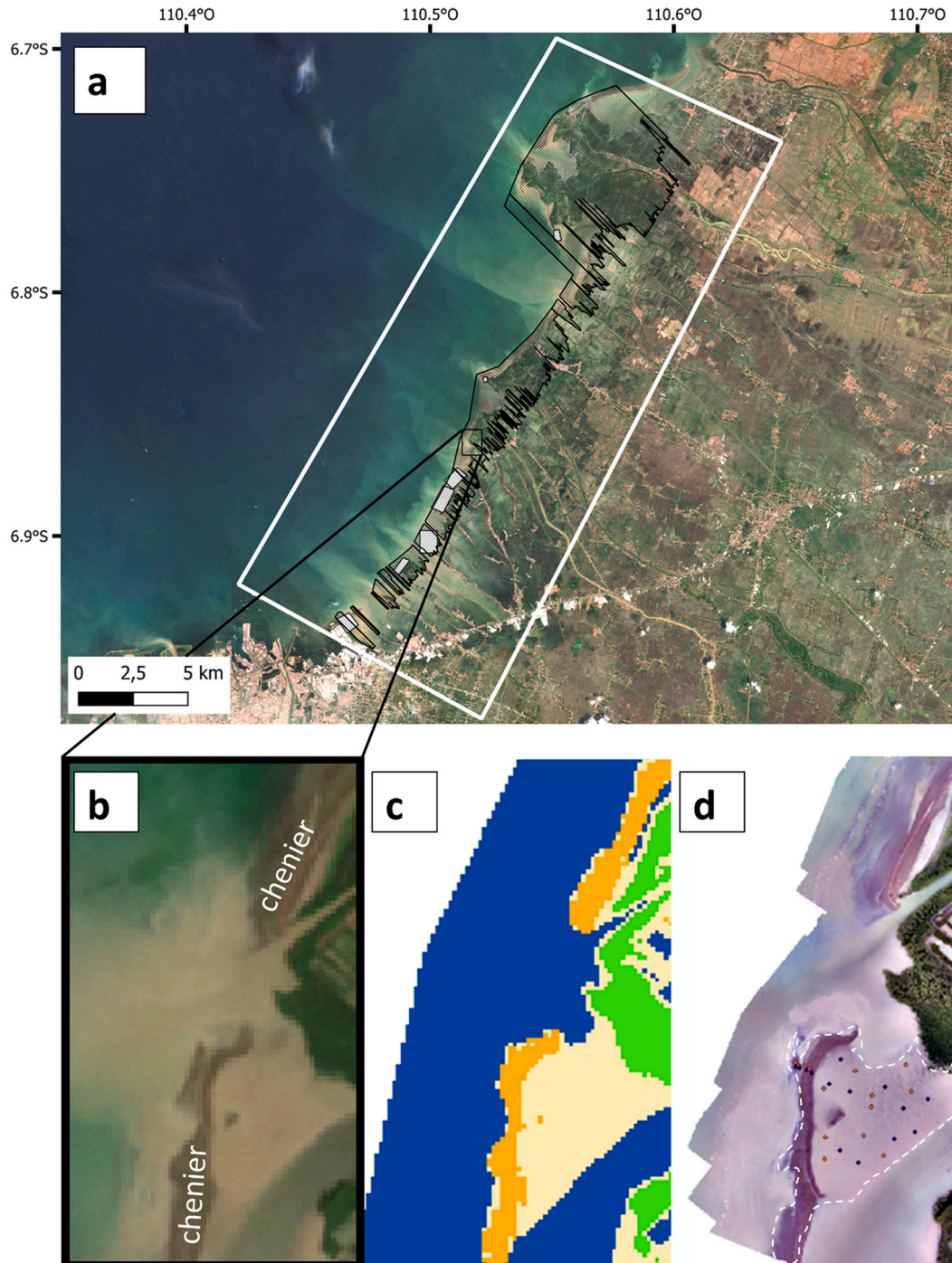


**Fig. 4.** Satellite image classification and validation to study mangrove response to chenier presence and mudflat width. **a.** The area of interest of the large scale and multi-temporal GIS study consisted of the area starting at every mangrove pixel at baseline (07-10-2015) until 2 km offshore (indicated with the black lined polygons). **b.** Close-up of a mangrove site featuring a mudflat and chenier on the RGB composite of one of the Sentinel-2 images of interest (15-11-2018, 02:59 UTC, water level: −30 cm rel. to MSL). **c.** Classified Sentinel-2 image showing the same close-up area with mangrove cover (green), mudflat (beige), sand (yellow) and water (blue). **d.** Drone image (6-11-2018, 08:47 UTC, water level: −15 cm rel. to MSL) of the field validation at this close-up site, with groundtruthing points on the chenier and mudflat and the outline of the emerged area during the drone flight. Another 7 validation sites were visited with the drone (indicated with the white filled rectangles in **a**). (For interpretation of the references to colour in this figure legend, the reader is referred to the web version of this article.)

**Table 1**

Error matrix resulting from sediment classification of exposed intertidal sediment in a Sentinel-2 image (November 15, 2018) and the sediment type observed in the field at 171 ground control points.

| | | Ground control data (known sediment types) | | | |
|---|---|---|---|---|---|
| | | Mud | Sand | Row total | |
| Classification data (from GIS) | Mud | 117 | 7 | 124 | User's accuracy Mud = 117/124 = 94% |
| | Sand | 8 | 39 | 47 | User's accuracy Sand = 39/ 47 = 83% |
| | **Column Total** | 125 | 46 | 171 | |
| | | **Producer's Accuracy** Mud = 117/125 = 94% | **Producer's Accuracy** Sand = 39 / 46 = 85% | | **Overall accuracy** = (117 + 39)/171 = 91% |

mangrove edge (Fig. 4a). Satellite images were then subjected to two steps of unsupervised classification, to cluster cells into four relevant classes in the study area: water, mud, sand and vegetation.

These four classes are easy to distinguish manually from the satellite imagery (Fig. 4b), but the differences in background reflection between the different dates made it difficult to use fixed thresholds of a certain band to distinguish these classes consistently between the dates. For instance, one spot in the middle of a mangrove stand can have an NDVI of 0.3 in the satellite image of one date and 0.7 on a different date, with mudflats having an NDVI of up to 0.5. Using a threshold of NDVI = 0.3 would therefore overestimate the mangrove cover on the second date, misclassifying sections of the mudflat as mangroves. To avoid this problem, we used an unsupervised classification tool (ArcGIS pro, Iso Cluster Unsupervised Classification Tool), which made it possible to automate the classification process for multiple images.

The tool uses a combination of an iterative self-organising (iso) algorithm (migrating means clustering) and a multivariate analysis of the input satellite bands to classify the raster cells based on their statistical similarity (maximum likelihood classification)(ESRI, 2020). When only one band was fed into the tool, the statistical method clustered the image in a way that was very similar to a clustering based on "natural jenks" in the frequency distribution. These tool-properties were used to classify the images in two steps (Fig. A 2). For the first step, the masked Sentinel-2 images were clustered into 5 groups using only the NDVI band as input for the unsupervised classification tool. One cluster was then classified as vegetation, two clusters were classified as exposed sediment (either wet or dry bed) and two clusters as water (either with moderate or high levels of suspended sediment) (Fig. A 3). The exposed sediment group was subsequently used in the second step of the classification. The exposed sediment layer per Sentinel-2 image was used as a mask for all 10 m and 20 m resolution bands per satellite image. These masked bands were then fed into the unsupervised classification tool, and subsequently clustered into a predefined number of sediment classes. Trial and error runs with various numbers of classes revealed that clustering the masked images into 8 groups consistently grouped "sand" into one class for all Sentinel-2 images (Fig. A 4). The signal of the "sand" cluster consistently showed a relatively high surface reflectance in the short wave infra-red (SWIR) bands in combination with a low to medium reflectance in the visible and near infrared bands, whereas the 7 mud clusters all showed a strong drop in surface reflectance between the near infrared and SWIR bands. This difference in SWIR reflectance between sand and mud is probably caused by the efficient drainage of sand in comparison to mud (Small et al., 2009). However, because we could not validate the different drainage levels of mud in the field, we added only the classes "sand" and "mud" to the first image classification resulting in a raster with classes: water, mud, sand and vegetation for every Sentinel image of interest (Fig. A 5).

*2.2.1.2. Validation of GIS classification.* To validate the unsupervised classification we visited 8 sites within the study area in October and November 2018 with a drone to collect a total of 171 ground control points with a dGPS and high resolution imagery of the cheniers, mud-flats and vegetation at low tide (Fig. 4d). Ground control points were classified as mud or sand in the field. These points were then used to

validate the sediment type as classified in the Sentinel image of November 2018. We determined the percentage of field stations that were classified correctly as sand and mud in GIS (the producer's accuracy), and we determined the percentage of test pixels from Sentinel-2 that were classified correctly based on the sediment type in the field (the user's accuracy (Table 1)). The user's accuracy showed that 94% of the ground control points that were classified as mud from the Sentinel-2 image were indeed muddy in the field, and that 83% of the locations that were classified as sand were indeed sandy in the field. Similarly, 94% of the sandy field locations were also classified as sandy based on the Sentinel-2 image and 85% of the muddy sites were classified as mud (Producer's Accuracy). Overall, the accuracy of the classification was 91% (kappa = 0.78, Lower 95%CI = 0.67, Upper 95%CI = 0.88).

*2.2.1.3. Definition of explanatory and response variables from GIS.* The classified Sentinel-2 images were used to quantify the effect of the presence/absence of cheniers on changes in mudflat cover and mangrove border along the dominant wind-direction during the monsoon season, which is north-west (MMAF, 2012). In order to obtain information along this direction, a total of 3255 north-west bearing lines were drawn from every cell that contained mangroves at baseline in October 2015 (the first selected Sentinel-2 image available) in the whole project area from Semarang to the Wedung Delta (Fig. 4a). Each bearing-line contained sampling points every 14.14 m, based on the diagonal width of the Seninel-2 raster cells. The feature classification was subsequently extracted at each sampling point from each date's classified raster with mangrove, mudflat, sand and water pixels. Bearing lines that contained clouds seaward of the mangrove border were excluded from further analysis.

Mangrove cover change between the acquisition dates was extracted from the classified images and used as the response variable. Mangrove cover change was categorized into one of three relevant response classes between two consecutive points in time: the classes being: "expanding", "stable", or "retreating" if the number of vegetation cells between the mangrove-sea border at $t_n$ and $t_{n+1}$ was respectively larger than -, equal to -, or less than zero.

To obtain chenier presence-absence data and mudflat data, the classified images were subjected to a smoothing algorithm according to van Bijsterveldt et al. (2020), which excluded small patches (10–20 m wide) of a certain category, such as ships (classified as sediment) in the water, or puddles of water on the mudflat. The smoothed classified Sentinel images were then used to extract shelter-related variables from the images such as, chenier presence and mud-flat width per bearing line for each of the selected acquisition dates. These characteristics were obtained by quantifying the number of cells of that class from the mangrove border in seaward direction along each bearing line and multiplying that number by the cell length 14.14 m.

*2.2.2. Data analysis*

*2.2.2.1. Hypothesis testing for the effect of cheniers and mudflats on mangroves.* To test the hypothesis that the presence of cheniers and mudflats drive mangrove border dynamics, we performed a linear regression separately on each of the three possible mangrove states

(retreat, stable or expanding). For these models, we decided only to include wet-season data because the largest changes related to mangrove cover were expected during this season; the propagule dispersal peak inducing mangrove expansion occurs at the start of the wet season (van Bijsterveldt et al., 2022), and the most impactful storms that could induce mangrove retreat occur during this season.

The response variable for each of the three models (mangrove expansion, stability and retreat) was the proportion of transects with that mangrove response occurring (e.g. mangrove retreat) for each unique combination of chenier stability and mean mudflat width. For example: mangrove retreat occurred in 33 out of 47 bearing lines without a chenier (0 years), and a mudflat width of 40 m wide. Mean mudflat width and chenier stability during the study period were thus added to each of the three linear regressions as explanatory variables. Chenier stability was defined as the number of years that a chenier had been present in a bearing line (0, 1 or ≥ 2 years). Mean mudflat width over the 4 wet seasons was log transformed and binned, to obtain groups of transects of similar size (a similar number of transects per unique mudflat width), to account for the log-normal distribution of mudflat widths (there were many transects with a small mudflat width and fewer transects with large mudflats).

## 3. Results

### 3.1. Field study: short-term cross-shore wave transformation with and without chenier

#### 3.1.1. Wave attenuation by cheniers

An offshore wavebuoy (12 km offshore in NW direction) revealed that waves during the field campaign arrived from a north-west direction (Fig. A 6), in line with each transect. The significant wave height (Hs) at the most seaward station of both transects was $0.5 \pm 0.2$ m on average during the field campaign, indicating that the boundary conditions during average wet season conditions of the two transects were comparable. The 8-day-averaged significant wave height (dashed line in Fig. 5) then dropped below $0.26 \pm 0.06$ m in both transects between the first two stations, where the foreshore of both transects was still comparable in terms of sediment composition (Fig. 3) and profile (Fig. 5). From there on, the wave height remained stable in the exposed transect, only showing a strong drop at the mangrove edge between station E4 (Hs: $0.24 \pm 0.06$ m) and station E5 (Hs: $0.15 \pm 0.08$ m), indicating that the waves break on the edge of the mangroves forest. This is further supported by Fig. A 8 (a), which shows a linear relationship between wave height and water depth at E5, characteristic of depth-limited wave
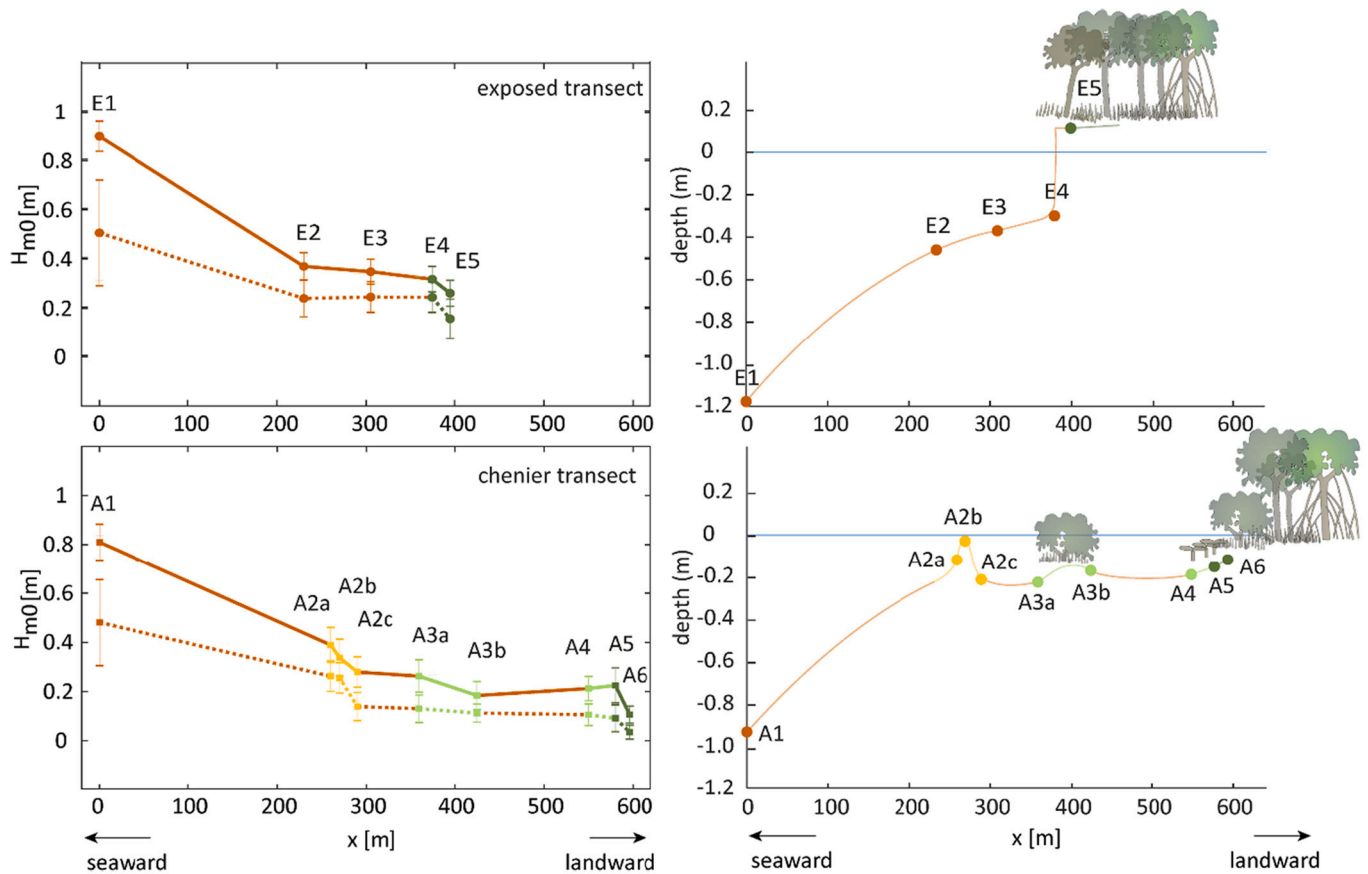


**Fig. 5.** Average significant wave height at each of the stations across the exposed transect and the chenier transect during storm conditions on the 1st of December (solid lines) and on average during the 8 days measured (dashed lines). NB: This graph only displays the wave transformation over the chenier when all stations were fully submerged simultaneously, thus when the chenier was also submerged. The location of each of the stations is indicated with colors relative to the colors of the schematized bathymetry profiles on the right. Depth was only measured at the stations and is displayed relative to mean water level during the campaign. The lines in between the stations are estimates of the profile contour.

breaking. In contrast, the waves in the chenier transect already showed a strong drop at the chenier stations A2a, A2b, and A2c (Hs: $0.26 \pm 0.06$, Hs: $0.26 \pm 0.06$, and Hs: $0.14 \pm 0.06$ resp.), indicating that the waves break on the chenier. All stations landwards from A2a thus display a linear relation between water levels and wave heights (Fig. A 8 b). This resulted in a significant wave height of $0.13 \pm 0.06$ m at the mangrove edge of the vegetated chenier (A3a) and waves of $0.11 \pm 0.04$ m at the edge of the main mangrove forest (A4) of the chenier transect under average wet season conditions. The significant wave height at both of these mangrove stations was significantly lower ($F = 229.9$, df = 2, $p < 0.0001$) than the waves at the mangrove border in the exposed transect (E4, Hs: $0.24 \pm 0.06$). The full time series of wave heights and water levels at all stations can be seen in Fig. A 6 and Fig. A 7.

### 3.1.2. Wave attenuation by cheniers under storm conditions

In addition to the average wet season conditions, we plotted the wave conditions measured on the first of December separately in Fig. 5. On this day, the instruments detected a significant increase in water level and significant wave height. This signal was caused by cyclone Dahlia passing nearby, along the south coast of Java. The cyclone increased the water level 60 cm above mean sea level (Alferink, 2022), and the flooding that followed was reported by villagers to be the worst flooding in the last 30 years. During this storm, the chenier had a similar effect on the waves, decreasing the significant wave height by >10 cm (from $0.39 \pm 0.07$ m to $0.28 \pm 0.06$ m). As a consequence, the significant wave heights at the mangrove edge of the vegetated chenier (Hs A3a: $0.26 \pm 0.07$) and the edge of the main forest of the chenier transect (Hs A4: $0.21 \pm 0.04$) were both significantly lower ($F = 12.94$, df = 2, $p < 0.0001$) than at the edge of the mangrove forest of the exposed transect (Hs E4: $0.32 \pm 0.05$). Further landward from the chenier, the wave height also decreased over the vegetated chenier (from $0.26 \pm 0.07$ m to $0.18 \pm 0.06$ m) and between the two stations inside the mangrove forest (from $0.23 \pm 0.07$ m to $0.11 \pm 0.03$ m). This illustrates how the canopy of the young, shrub-like, trees are able to cause further

wave attenuation during the high water levels of a storm.

### 3.1.3. Forest characteristics behind cheniers

The forest characteristics at the most landward stations were very different for both transects (Table 2); the chenier transect had a high seedling density of the two common *Avicennia* species in the area (*Avicennia alba* and *Avicennia marina*), whereas no seedlings of these species were found in the exposed transect. In the exposed transect, 20% of the mature trees were dead, mostly occurring at the edge, indicating mangrove retreat as a result of erosion. Saplings were completely absent from both forest plots, indicating that seedlings that had established before the wet season of 2017–2018 had not survived.

### 3.2. GIS study: the relation between intertidal foreshore features and mangrove dynamics

#### 3.2.1. The multi-year net effect of cheniers and mudflats on mangrove dynamics

The probability of mangrove expansion on a larger scale and over multiple years in relation to the presence of cheniers and the width of mudflats was investigated using linear regression. Both mean mudflat width and chenier stability proved to have a significantly positive impact on mangrove expansion ($F = 33.1$, df = 2 & 58, $R^2 = 0.52$, $p < 0.001$). The probability of mangrove retreat decreased significantly with larger mudflat widths and more stable cheniers ($F = 77.6$, df = 2 & 58, $R^2 = 0.72$, $p < 0.001$). The proportion of stable mangrove fringes was small under all foreshore conditions, indicating that mangroves tend to be dynamic, switching between a state of expansion or retreat, although mudflat width did have a positive effect on mangrove stability ($F = 22.56$, df = 2 & 58, $R^2 = 0.42$, $p < 0.001$). Plotting the observed probabilities of each mangrove state shows that without a chenier and the smallest observed mudflat, the probability that mangroves retreated was much higher (70%) than the chance that they were stable (13%) or expanding (17%) (Fig. 6). However, mangrove forest retreat clearly

**Table 2**
Forest parameters at the most landward stations of the exposed and chenier transects after the wet season in 2017–2018.

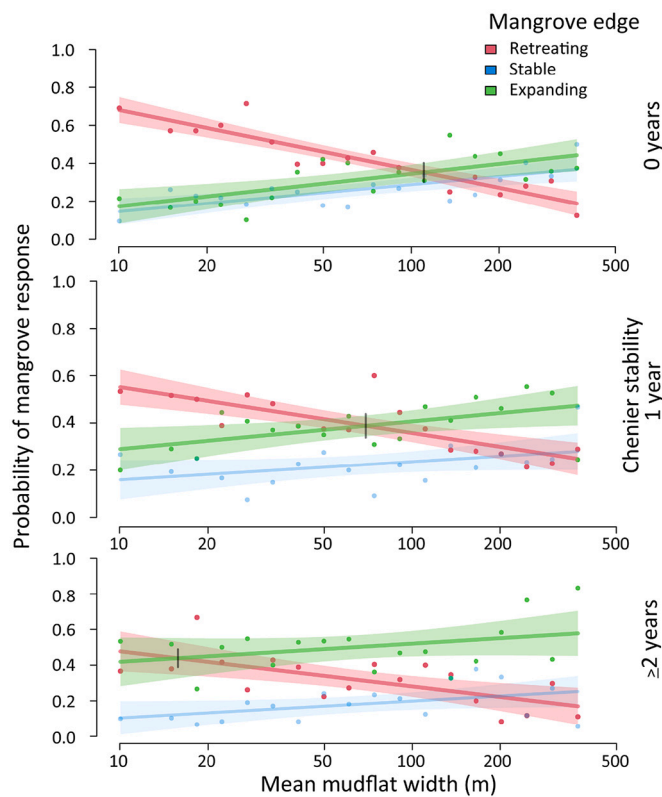| Transect | Species | Seedling Density (ha$^{-1}$) | Sapling Density (ha$^{-1}$) | Tree Density (ha$^{-1}$) | Tree DBH ($\pm$SD) (cm) | Tree Mortality (% of dead trees) |
|---|---|---|---|---|---|---|
| chenier | A. marina | 42,116 | 0 | 260 | 0.3 (0) | 0 |
| | R. mucronata | 0 | 0 | 260 | 1.0 (0) | 0 |
| | A. alba | 3120 | 0 | 1040 | 2.4 (2.1) | 0 |
| | **Total** | **45,236** | **0** | **1560** | | |
| exposed | A. marina | 0 | 0 | 1274 | 10.2 (6.6) | 20 |
| | R. mucronata | 0 | 382 | 1529 | 1.7 (0.8) | 0 |
| | A. alba | 0 | 0 | 0 | | |
| | **Total** | **0** | **382** | **2803** | | |

**Fig. 6.** Probability and 95% confidence intervals of mangrove response (retreat, stable or expansion) in relation to mean mudflat width (m, in bins) for various degrees of chenier stability (the number of years a chenier was present per transect) during the 4 year time frame of the study. The mean mudflat width required to make mangrove expansion more likely than mangrove retreat is indicated with a black vertical line in each panel.

decreased with an increase in mudflat width, even in the absence of a chenier (chenier stability = 0 years). Without a chenier, mangroves were more likely to expand than retreat from a mudflat width of 110 m onward (95% CI: 76–183 m). This tipping point between mangrove retreat and mangrove expansion occurred at smaller mudflat widths when a chenier was present offshore. When a chenier was stable for one year in front of the mangrove fringe, a mudflat width of only 70 m (95% CI: 35–145 m) was needed to flip the odds in favor of mangrove expansion. When a chenier had been present for two years or longer, this tipping point occurred at a mudflat width of 16 m (95% CI: 0–43 m). Therefore, the more stable a chenier, the larger the chances of mangrove expansion (Fig. 6).

## 4. Discussion

In this study, we investigated the effect of both *i)* cheniers and *ii)* intertidal mudflat width on mangrove dynamics, using *i)* wave measurements at cross-shore transects in the field and *ii)* multi-year satellite data on mangrove dynamics. Our field data show that existing cheniers reduce the height of the waves arriving at the mangrove fringe, thereby creating a shelter for mangroves as long as the chenier is present. Our GIS data confirm that the temporary shelter created by cheniers increases the chances of net mangrove expansion and reduces the occurrence of mangrove retreat. In the absence of cheniers, a much wider intertidal mudflat is required to facilitate mangrove expansion.

### 4.1. Local chenier effects: wave reduction and habitat creation

The fact that offshore cheniers reduce the wave height at the mangrove fringe is in itself not unexpected. In sandy systems, sand banks

and barrier islands are well known to cause wave height reduction at the shoreline (Short, 2001). However, the mechanism of wave height reduction over sandy offshore features is different from wave height reduction over muddy foreshores. Muddy foreshores cause wave attenuation due to bottom friction caused by sediment resuspension and the absorbing effect of the liquid mud top layer (Sheremet and Stone, 2003), whereas the relatively steep and hard surface of sandy foreshores cause waves to break (Short, 2001; Wolf et al., 2011). These two wave reducing processes are seemingly combined in the case of sandy cheniers atop of a muddy foreshore, where wave height is reduced over the muddy foreshore (from A1 to A2a and from E1 to E2 in Fig. 5), before breaking on top of the sandy chenier (A2a-A2c, Fig. 5). The difference between the storm conditions and average wet season furthermore show how the effect of the chenier is influenced by the water depth. When a chenier is fully emerged during low tide it acts as a barrier, and the water surface on the landward side of the chenier is completely still (e.g. Fig. 1 Field site picture). When a chenier is submerged, for instance during the measured wet-season conditions (dashed lines in Fig. 5), the chenier reduces the wave height (in this case by 10 cm). The absolute amount of wave reduction by the studied chenier remained the same (±10 cm) when the water level peaked during the storm of the 1st of December. However, proportionally the wave height reduction over the chenier was smaller during the storm, as the incoming waves were larger, ultimately allowing significantly larger waves to reach the mangrove edge. The chenier that was measured during this field campaign was relatively low in elevation. Cheniers can be dynamic both in position and height, as was demonstrated for a different chenier in our study area by Tas et al. (2020). A larger and higher chenier would be emerged from the water for longer periods of time during the day, and thus provide a more effective shelter from waves for the mangroves behind it than a smaller and lower chenier. Nevertheless, the field data show that even submerged cheniers have a clear sheltering effect on existing mangroves.

The relatively calm backwater that is created by cheniers affects both mudflats and mangroves. The low wave height that was measured directly landward of the chenier in this field study is favorable for deposition of small sediment particles. The high silt content (Fig. 3) and the soft quality of the mud that were observed landward of the chenier (Table 2 picture) indeed suggest that cheniers facilitate mudflat formation in the area that they shelter. Mudflats in their own right are known to have a protective (Bouma et al., 2016; van Bijsterveldt et al., 2020) and nursing role (Swales et al., 2007) towards mangroves. Unfortunately, the size of intertidal areas has been declining on a global scale over the last 30 years as a result of, among others, coastal development, decreased sediment input, and increased drainage and compaction (Murray et al., 2019). The few tropical sites that show an expansion of intertidal area, also display a seaward migration of mangroves (Murray et al., 2019), illustrating the importance of a sizable intertidal area for mangrove development. Our GIS results showed that the likelihood of mangrove expansion indeed increased significantly with increasing size of intertidal mudflats, with mangrove expansion becoming more likely than mangrove die-back from an intertidal mudflat size of 110 m (95% CI: 76–183 m) onward in this microtidal system. In macrotidal systems the necessary intertidal mudflat width to support mangrove expansion might be larger, as deeper water at high tide allows for higher waves to reach the shoreline, though intertidal areas tend to be wider in such systems as well (Murray et al., 2019). Nevertheless, one third of the world's tropical mangroves can be categorized as micro-tidal and sedimentary (Balke and Friess, 2016), like the coastline of Demak. Therefore, the tipping points in mangrove expansion in relation to mudflat width found in this study could potentially be helpful in management of other micro-tidal mangrove forests around the globe as well.

*4.2. Large-scale and long-term chenier effects: the importance of a calm wet season*

The data in this study revealed that the presence of a wide mudflat or the presence of a chenier can support net mangrove expansion over multiple years. However, this does not mean that the presence of a chenier or mudflat during a wet season necessarily results in mangrove expansion during that fruiting season. The latter requires also a Window of Opportunity to occur, consisting of an inundation-, wave-and erosion-free period to strand, root and anchor themselves, and thereby survive the first life stages (Balke et al., 2011). In the field, the forest characteristics at the most landward edge of the chenier transect showed that there had been no window of opportunity for mangrove growth during the previous season, because saplings were completely absent from the site. The absence of saplings, while seedlings were abundant, suggests that the seedlings that had established at the start of the wet season (and would have grown into saplings before this field campaign) did not survive this particular storm season. This observation indicates that, while cheniers and mudflats reduce wave height and promote mudflat accretion, successful mangrove establishment in the seaward direction remains an event-driven process.

Satellite analyses support that the colonization of mangrove habitat occurs episodically and is therefore non-linear through time. Net mangrove expansion occurred primarily during only one wet season (2016–2017: A 5). During this wet season, a Window of Opportunity probably occurred due to the remarkably low maximum daily wind speeds of ±10 m/s (as retrieved from the Ahmand Yani airport station in Semarang (http://dataonline.bmkg.go.id/data_iklim). Thereby the dry-season-like wind speeds, though in onshore direction, coincided with the fruiting season of the common *Avicennia* species in the area, blowing the propagules towards the shore. The combination of available propagules and the presence of wide mudflats for establishment, followed by months of calm conditions were likely the cause of the positive mangrove cover change during that same season. This combination of favorable conditions resulted in a staircase-like appearance of the forest-canopy (e.g. Fig. 3d in van Bijsterveldt et al., 2020), caused by separated events of mangrove expansion interspaced by years of non-expansion. Non-linearity in seaward mangrove expansion is not uncommon, and has also described in the coastal system of the Guianas in South America, where migrating mud banks offer temporary shelter and habitat for mangrove expansion, interspaced with decades of non-shelter and non-expansion (e.g. Fig. 11 in Anthony et al., 2010). Similar periodic mangrove expansion, though by a different mechanism, has been observed in the Firth of Thames, New Zealand, where reduced wind and wave energy during the El Niño events of 1978–1981 and 1991–1995 resulted in two major seaward forest expansion events (Lovelock et al., 2010). Our findings therefore illustrate how seaward mangrove expansion can be induced by a combination of temporal shelter and temporal calm conditions.

*4.3. Management implications*

The observation that cheniers create temporary shelter for mangroves from waves, especially when they are stable over longer periods of time, has implications for mangrove conservation and restoration. For example, despite their role in mangrove establishment, cheniers have been mined to use their sand for construction in Demak, which deprives the coastline from their erosion mitigation function. Sand mining should thus be strictly regulated to maximize mangrove colonization and mitigate retreat. Conversely, mangrove persistence and expansion could be favored if existing cheniers are stabilized or supplied with sand from a sustainable source. Although artificial sand nourishments have been used as wave breakers before (e.g. Hwung et al., 2010), little is known about sand nourishments on muddy substrate, presumably because sand is relatively rare along muddy coasts. The tipping points for mangrove retreat at specific mudflat widths also have useful, and perhaps more

feasible, implications for management. For instance, satellite imagery of low tide conditions or the use of a tidal flat change map as presented in Murray et al. (2019) (http://intertidal.app), could help coastal managers to assess the width of the existing intertidal foreshore along the coastline and identify locations where the mudflat width is low or decreasing rapidly. Those locations could then be targeted with foreshore modification methods, such as nourishments (Baptist et al., 2019) or the erection of brushwood dams or fences, which are placed parallel to the coastline to trap sediment. The latter method has proven to be particularly effective along muddy shorelines (Winterwerp et al., 2020). So far, these structures have been intended to elevate mudflats high enough (> MSL) to restore mangrove habitat (Mancheño et al., 2022), but the insights gained in this study show that restoration of lower elevation mudflats could already be worthwhile to reduce the chances of mangrove retreat. Foreshore modifications that create wide intertidal foreshores may thus be useful measures to ascertain that wave-attenuating ecosystems such as salt marshes and mangroves become stable enough to be utilized in coastal protection schemes.

## Data availability

Data in support of this manuscript are available at https://doi.org/10.4121/21667685.

Wesenbeeck and Han Winterwerp for the many fruitful discussions on chenier dynamics and chenier-mangrove interactions.

## Appendix A. Appendices



**A 1 A.** Consolidated mud with cliff formation ($+/-$ 10 cm) around the breaker zone at the seaward edge of the chenier before placement of station A2a. **B.** Sand to consolidated mud transition. Note how the footsteps get deeper towards the seaward edge of the chenier, where the sand layer on top of the mud becomes thinner. **C.** Picture direction of A and B, and a series of transparent cores taken on the seaward side of the chenier transect in the dry season prior to this study. Note how all cores contain a layer of sand (white lines), and below that, a muddy layer with intermixed layers of sand (dashed lines). The most seaward core and the core closest to the chenier also contain a thick layer of mud (black) on top of the mixed layers.
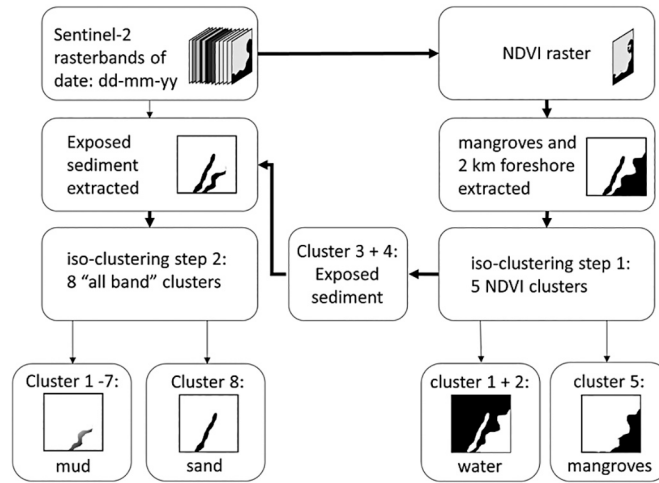
**A 2** Flow chart of the steps for unsupervised classification of all Sentinel-2 images of dates of interest between 2015 and 2019 in 4 relevant classes (water, mud, sand and mangroves).
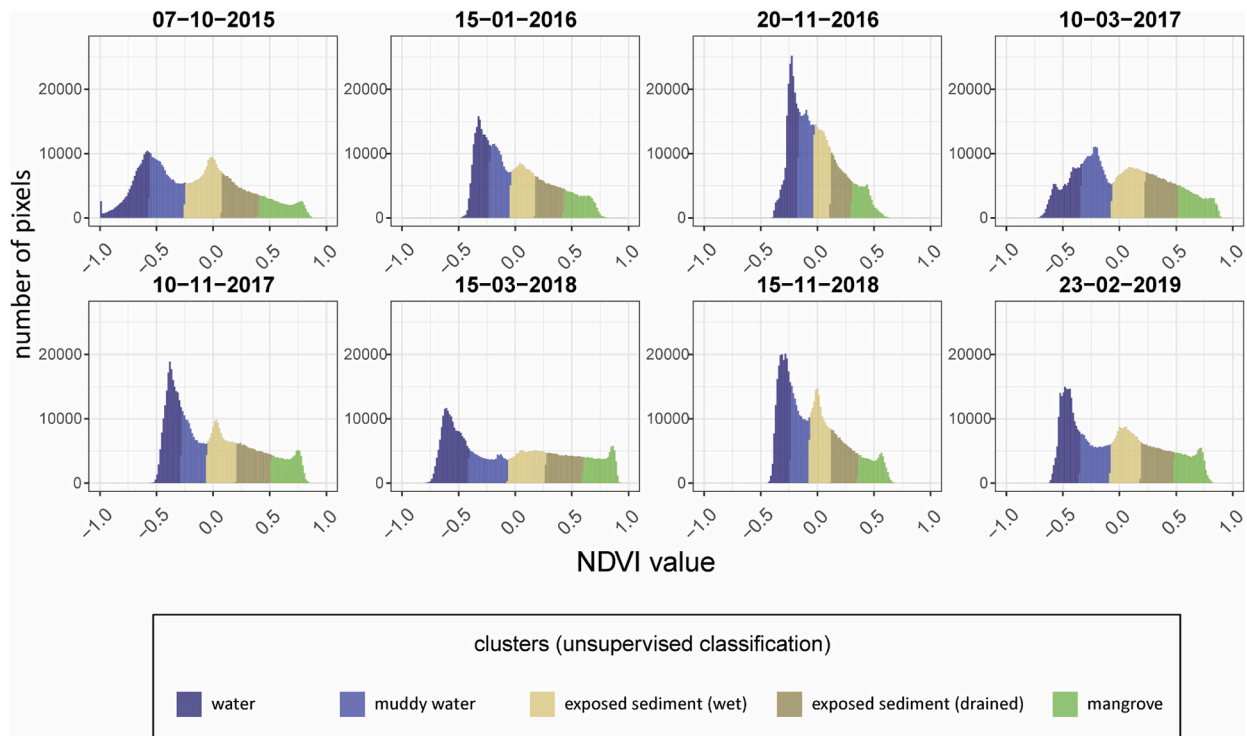


A 3 Histograms showing the number of pixels that were clustered into one of the 5 classes by the isocluster unsupervised classification tool based on maximum likelihood clustering of the NDVI rasters computed from each of the Sentinel-2 satellite images.
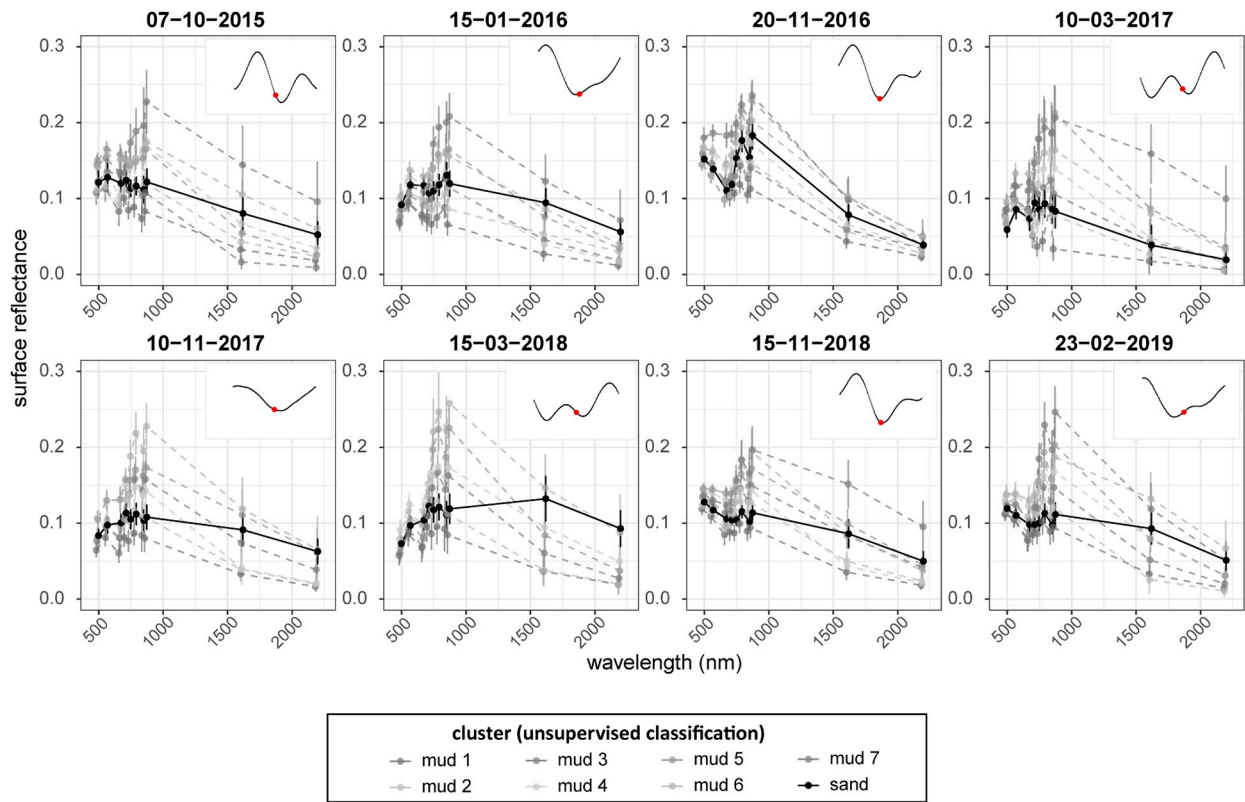
**A 4** Spectral signals of each of the 8 clusters produced by the unsupervised classification step. The sand cluster distinguishes itself from the "mud" clusters by relatively high surface reflectance values in the SWIR bands (wavelength > 900 nm) and low to average reflectance in the visible (wavelength < 700 nm) and the near infrared spectrum (wavelength: 700–900 nm). The tidal stage at the time and date of image acquisition is indicated with a red dot within the tidal cycle of that date in the upper right corner of each panel.
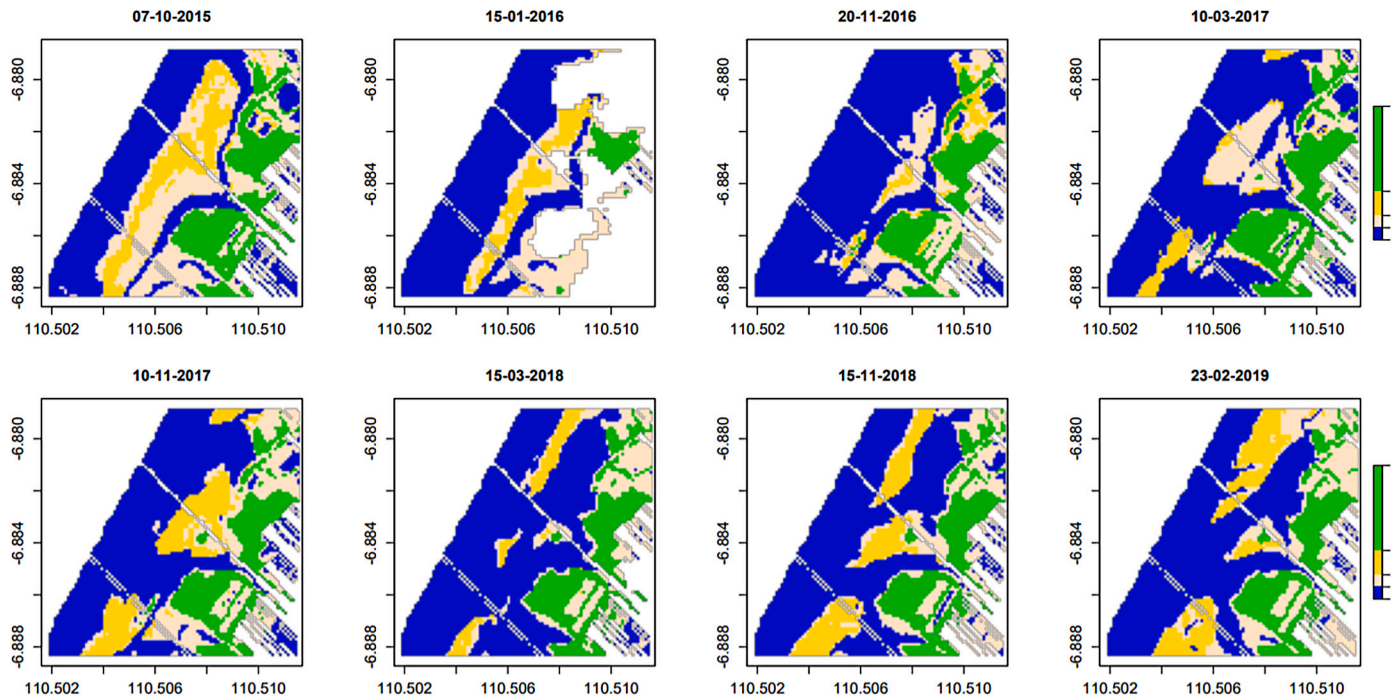


**A 5** NW bearing lines along which the information of the classified Sentinel-2 images is displayed, with mangroves (green), water (blue), mud (beige) and sand (yellow). These classified images are zoomed in on the site where the two field transects were deployed in November 2017.
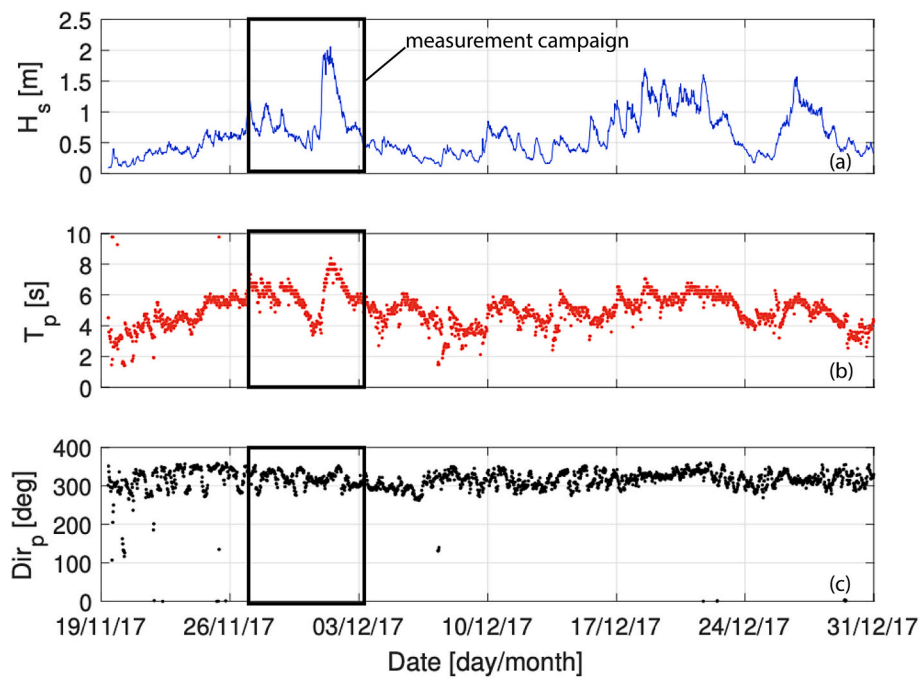
**A 6** Time series of significant wave height (a), peak wave period (b), and wave direction (c) from an offshore buoy (Wave Droid) during the measurement campaign (shown with a black rectangle). Source: (Van Domburg, 2018).
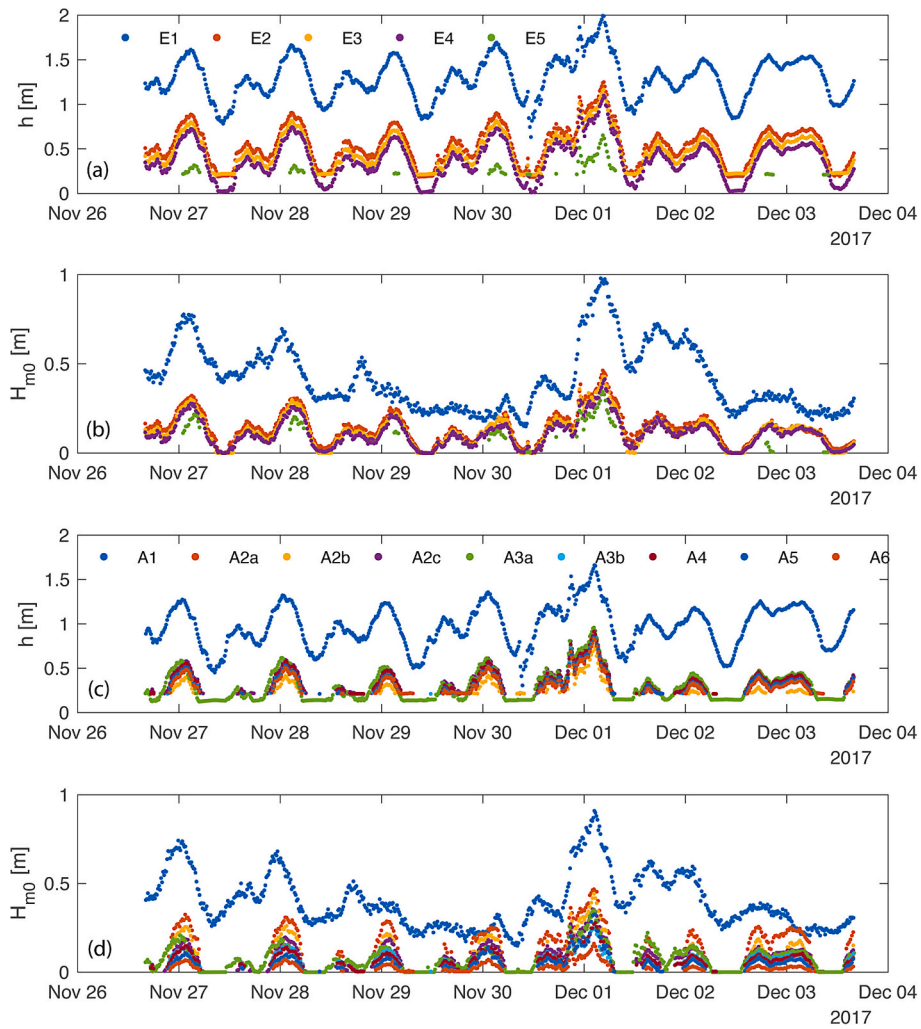
**A 7** Time series of the water depth in (a) the exposed transect, and (c) the chenier transect. Time series of the wave height in (b) the exposed transect, and (d) the chenier transect.
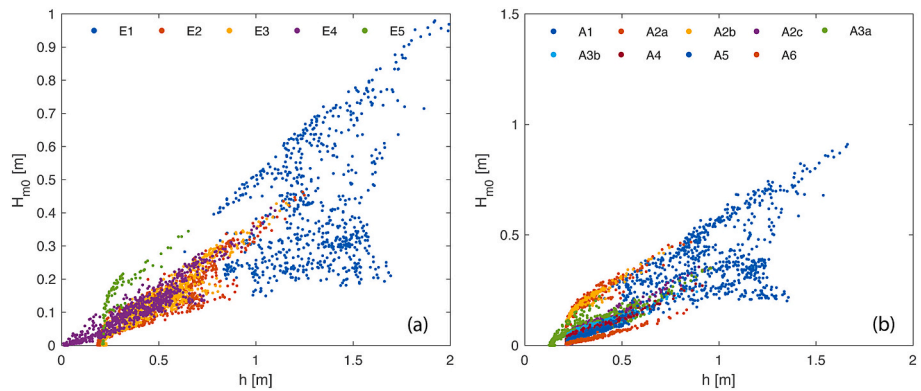


**A 8** Ratio of significant wave height to water depth at (a) exposed transect and (b) chenier transect.

# References

Afifah, S., Hizbaron, D.R., 2020. Vulnerability assessment of residential buildings to tidal flood hazards in Sriwulan Village, Sayung District, Demak Regency. E3S Web Conf 200. https://doi.org/10.1051/e3sconf/202020001008.

Alferink, M., 2022. Wave Transmission through Permeable Structures in Demak Indonesia. Delft University of Technology.

Anthony, E.J., 1989. Chenier plain development in northern Sierra Leone, West Africa. Mar. Geol. 90, 297–309. https://doi.org/10.1016/0025-3227(89)90132-1.

Anthony, E.J., Gardel, A., Gratiot, N., Proisy, C., Allison, M.A., Dolique, F., Fromard, F., 2010. The Amazon-influenced muddy coast of South America: a review of mud-bank–shoreline interactions. Earth-Science Rev 103, 99–121. https://doi.org/10.1016/j.earscirev.2010.09.008.

Anthony, E.J., Brunier, G., Gardel, A., Hiwat, M., 2019. Chenier morphodynamics on the amazon-influenced coast of suriname, South America: Implications for beach ecosystem services. Front. Earth Sci. 7, 1–20. https://doi.org/10.3389/feart.2019.00035.

Augustinus, P.G.E.F., 1978. The Changing Shoreline of Surinam(South America). Utrecht University.

Augustinus, P.G.E.F., 1989. Cheniers and chenier plains: a general introduction. Mar. Geol. 90, 219–229. https://doi.org/10.1016/0025-3227(89)90126-6.

Balke, T., Friess, D.A., 2016. Geomorphic knowledge for mangrove restoration: a pan-tropical categorization. Earth Surf. Process. Landf. 41, 231–239. https://doi.org/10.1002/esp.3841.

Balke, T., Bouma, T.J., Horstman, E.M., Webb, E.L., Erftemeijer, P.L., Herman, P.M.J., 2011. Windows of opportunity: Thresholds to mangrove seedling establishment on tidal flats. Mar. Ecol. Prog. Ser. 440, 1–9. https://doi.org/10.3354/meps09364.

Bao, T.Q., 2011. Effect of mangrove forest structures on wave attenuation in coastal Vietnam. Oceanologia 53, 807–818. https://doi.org/10.5697/oc.53-3.807.

Baptist, M.J., Gerkema, T., van Prooijen, B.C., van Maren, D.S., van Regteren, M., Schulz, K., Colosimo, I., Vroom, J., van Kessel, T., Grasmeijer, B., Willemsen, P., Elschot, K., de Groot, A.V., Cleveringa, J., van Eekelen, E.M.M., Schuurman, F., de Lange, H.J., van Puijenbroek, M.E.B., 2019. Beneficial use of dredged sediment to enhance salt marsh development by applying a 'Mud Motor'. Ecol. Eng. 127, 312–323. https://doi.org/10.1016/J.ECOLENG.2018.11.019.

Barbier, E.B., Hacker, S.D., Kennedy, C., Koch, E.W., Stier, A.C., Silliman, B.R., 2011. The value of estuarine and coastal ecosystem services. Ecol. Monogr. 81, 169–193.

Bouma, T.J., van Belzen, J., Balke, T., van Dalen, J., Klaassen, P., Hartog, A.M., Callaghan, D.P., Hu, Z., Stive, M.J.F., Temmerman, S., Herman, P.M.J., 2016. Short-term mudflat dynamics drive long-term cyclic salt marsh dynamics. Limnol. Oceanogr. 0, 1–15. https://doi.org/10.1002/lno.10374.

Cangzi, Liu, Walker, H.J., 1989. Sedimentary characteristics of cheniers and the formation of the Chenier Plains of East China. J. Coast. Res. 5, 353–368.

Chapman, V.J., 1976. Wet Coastal Ecosystems. Elsevier scientific publishing company, Amsterdam.

Duarte, C.M., Losada, I.J., Hendriks, I.E., Mazarrasa, I., Marbà, N., 2013. The role of coastal plant communities for climate change mitigation and adaptation. Nat. Clim. Chang. 3, 961–968. https://doi.org/10.1038/nclimate1970.

ESRI, 2020. Iso Cluster Unsupervised Classification [WWW Document]. Tool Ref. Spat. Anal. Toolbox, Multivar. Toolset. URL https://desktop.arcgis.com/en/arcmap/latest/tools/spatial-analyst-toolbox/iso-cluster-unsupervised-classification.htm.

Horstman, E.M., Dohmen-Janssen, C.M., Narra, P.M.F., van den Berg, N.J.F., Siemerink, M., Hulscher, S.J.M.H., 2014. Wave attenuation in mangroves: a quantitative approach to field observations. Coast. Eng. 94, 47–62. https://doi.org/10.1016/j.coastaleng.2014.08.005.

Hwung, H.-H., Huang, Z.-C., Hwang, K.-S., 2010. An experimental study of the cross-shore evolution of artificial submerged sand bars. Coast. Eng. J. 52, 261–285. https://doi.org/10.1142/S057856341000221X.

Lovelock, C.E., Sorrell, B.K., Hancock, N., Hua, Q., Swales, A., 2010. Mangrove forest and soil development on a rapidly accreting shore in New Zealand. Ecosystems 13, 437–451. https://doi.org/10.1007/s10021-010-9329-2.

Mancheño, A.G., Reniers, A.H.M.J., van Wesenbeeck, B.K., van Bijsterveldt, C.E.J., Tas, S., Wilms, T., Muskanonfola, M., Winterwerp, J.C., 2022. Restoring Eroding Mangrove Coastlines using Nature-Based Structures (in Preparation for Submission).

Mazda, Y., Magi, M., Kogo, M., Hong, P.N., 1997. Mangroves as coastal protection from waves in the Tong King delta, Vietnam. Mangrove Salt Marshes. https://doi.org/10.1023/A:1009928003700.

Mazda, Y., Magi, M., Ikeda, Y., Kurokawa, T., Asano, T., 2006. Wave reduction in a mangrove forest dominated by Sonneratia sp. Wetl. Ecol. Manag. 14, 365–378. https://doi.org/10.1007/s11273-005-5388-0.

McBride, R.A., Taylor, M.J., Byrnes, M.R., 2007. Coastal morphodynamics and Chenier-Plain evolution in southwestern Louisiana, USA: a geomorphic model. Geomorphology 88, 367–422. https://doi.org/10.1016/j.geomorph.2006.11.013.

MMAF, 2012. Oceanography Condition in Coastal of Sayung Sub-District, District of Demak. Province of Central Java.

Murray, N.J., Phinn, S.R., DeWitt, M., Ferrari, R., Johnston, R., Lyons, M.B., Clinton, N., Thau, D., Fuller, R.A., 2019. The global distribution and trajectory of tidal flats. Nature 565, 222–225. https://doi.org/10.1038/s41586-018-0805-8.

Narayan, S., Beck, M.W., Reguero, B.G., Losada, I.J., Van Wesenbeeck, B., Pontee, N., Sanchirico, J.N., Ingram, J.C., Lange, G.M., Burks-Copes, K.A., 2016. The effectiveness, costs and coastal protection benefits of natural and nature-based defences. PLoS One 11, 1–17. https://doi.org/10.1371/journal.pone.0154735.

Othman, M.A., 1994. Value of mangroves in coastal protection. Hydrobiologia 285, 277–282. https://doi.org/10.1007/BF00005674.

Prost, M.T., 1989. Coastal dynamics and chenier sands in French Guiana. Mar. Geol. 90, 259–267.

Quartel, S., Kroon, A., Augustinus, P.G.E.F., Van Santen, P., Tri, N.H., 2007. Wave attenuation in coastal mangroves in the Red River Delta, Vietnam. Vietnam J Asian Earth Sci 29, 576–584. https://doi.org/10.1016/j.jseaes.2006.05.008.

Russell, R.J., Howe, H.V., 1935. Cheniers of Southwestern Louisiana. Geogr. Rev. 25, 449–461.

Sheremet, A., Stone, G.W., 2003. Observations of nearshore wave dissipation over muddy sea beds. J. Geophys. Res. 108, 3357. https://doi.org/10.1029/2003JC001885.

Short, A.D., 2001. Beaches, Physical Processes Affecting*. In: Steele, J.H. (Ed.), Encyclopedia of Ocean Sciences, Second edition. Academic Press, Oxford, pp. 305–315. https://doi.org/10.1016/B978-012374473-9.00084-9.

Small, C., Steckler, M., Seeber, L., Akhter, S.H., Goodbred, S., Mia, B., Imam, B., 2009. Spectroscopy of sediments in the Ganges-Brahmaputra delta: Spectral effects of moisture, grain size and lithology. Remote Sens. Environ. 113, 342–361. https://doi.org/10.1016/j.rse.2008.10.009.

Spalding, M.D., Ruffo, S., Lacambra, C., Meliane, I., Hale, L.Z., Shepard, C.C., Beck, M.W., 2014. The role of ecosystems in coastal protection: Adapting to climate change and coastal hazards. Ocean Coast. Manag. 90, 50–57. https://doi.org/10.1016/j.ocecoaman.2013.09.007.

Swales, A., Bentley, S.J., Lovelock, C., Bell, R.G., 2007. Sediment processes and mangrove-habitat expansion on a rapidly-prograding muddy coast. New Zealand 40926, 1441–1454. https://doi.org/10.1061/40926(239)111.

Tas, S.A.J., van Maren, D.S., Reniers, A.J.H.M., 2020. Observations of cross-shore chenier dynamics in Demak, Indonesia. J Mar Sci Eng 8, 1–18. https://doi.org/10.3390/jmse8120972.

Temmerman, S., Meire, P., Bouma, T.J., Herman, P.M.J., Ysebaert, T., De Vriend, H.J., 2013. Ecosystem-based coastal defence in the face of global change. Nature 504, 1–5. https://doi.org/10.1038/nature12859.

van Bijsterveldt, C.E.J., 2015. MSc Thesis: Natural Mangrove Restoration, how Can it Be Induced? - Environmental Factors Regulating Natural Mangrove Establishment in an Eroding Aquaculture Area in Demak, Indonesia.

van Bijsterveldt, C.E.J., van Wesenbeeck, B.K., van der Wal, D., Afiati, N., Pribadi, R., Brown, B., Bouma, T.J., 2020. How to restore mangroves for greenbelt creation along eroding coasts with abandoned aquaculture ponds. Estuar. Coast. Shelf Sci. 235, 106576 https://doi.org/10.1016/j.ecss.2019.106576.

van Bijsterveldt, C.E.J., Debrot, A.O., Bouma, T.J., Maulana, M.B., Pribadi, R., Schop, J., Tonneijck, F.H., van Wesenbeeck, B.K., 2022. To plant or not to plant: when can planting facilitate mangrove restoration? Front Environ Sci 88, 18. https://doi.org/10.3389/fenvs.2021.690011.

Van Domburg, T., 2018. Identifying Windows of Opportunity for Mangrove Establishment on a Mud Coast. Delft University of Technology.

Van Maren, D.S., 2005. Barrier formation on an actively prograding delta system: the Red River Delta. Vietnam Mar Geol 224, 123–143. https://doi.org/10.1016/j.margeo.2005.07.008.

Winterwerp, J.C., Albers, T., Anthony, E.J., Friess, D.A., Mancheño, A.G., Moseley, K., Muhari, A., Naipal, S., Noordermeer, J., Oost, A., Saengsupavanich, C., Tas, S.A.J., Tonneijck, F.H., Wilms, T., Van Bijsterveldt, C., Van Eijk, P., Van Lavieren, E., Van Wesenbeeck, B.K., 2020. Managing erosion of mangrove-mud coasts with permeable dams – lessons learned. Ecol. Eng. 158, 106078 https://doi.org/10.1016/j.ecoleng.2020.106078.

Wolf, J., Brown, J.M., Bolaños, R., Hedges, T.S., 2011. 2.10 - waves in coastal and estuarine waters. In: Wolanski, E., McLusky, D. (Eds.), Treatise on Estuarine and Coastal Science. Academic Press, Waltham, pp. 171–212. https://doi.org/10.1016/B978-0-12-374711-2.00203-5.

Woodroffe, C.D., Grime, D., 1999. Storm impact and evolution of a mangrove-fringed chenier plain, Shoal Bay, Darwin. Australia Mar Geol 159, 303–321. https://doi.org/10.1016/S0025-3227(99)00006-7.